

V2X Sidelink Positioning in FR1: From Ray-Tracing and Channel Estimation to Bayesian Tracking

Yu Ge*, Maximilian Stark†, Musa Furkan Keskin*, Hui Chen*,

Guillaume Jornod†, Thomas Hansen†, Frank Hofmann†, Henk Wymeersch*

*Department of Electrical Engineering, Chalmers University of Technology, Gothenburg, Sweden,

†Robert Bosch GmbH, Hildesheim, Germany

Abstract—Sidelink positioning research predominantly focuses on the snapshot positioning problem, often within the mmWave band. Only a limited number of studies have delved into vehicle-to-anything (V2X) tracking within sub-6 GHz bands. In this paper, we investigate the V2X sidelink tracking challenges over sub-6 GHz frequencies. We propose a Kalman-filter-based tracking approach that leverages the estimated error covariance lower bounds (EECLBs) as measurement covariance, alongside a gating method to augment tracking performance. Through simulations employing ray-tracing data and super-resolution channel parameter estimation, we validate the feasibility of sidelink tracking using our proposed tracking filter with two novel EECLBs. Additionally, we demonstrate the efficacy of the gating method in identifying line-of-sight paths and enhancing tracking performance.

Index Terms—V2X, sidelink tracking, sub-6 GHz, EECLB, measurement covariance, gating, ray-tracing.

I. INTRODUCTION

Integrated sensing and communication (ISAC) has garnered significant attention in the evolution of 5G mobile radio systems and emerges as a cornerstone feature in beyond 5G communication systems [1], [2]. Many studies have focused on the mmWave bands, primarily due to their larger available bandwidth at higher carrier frequencies, leading to enhanced time-delay resolution [3], [4]. Lower bands, such as the sub-6 GHz bands, also hold significant promise for sensing applications, particularly in environments with less complicated multipath propagation [5]. One notable application is vehicle-to-anything (V2X) communication [6], where radio sensing supports various driving functions aimed at improving passenger safety and comfort [7]. Within V2X, sidelink communication can effectively utilize the 5850-5925 MHz band at frequency range 1 (FR1), along with neighboring unlicensed bands, to bolster sensing capabilities [8], [9], thereby enhancing integrity, accuracy, and power efficiency [10]. As lower bands are expected to be more widely used for sidelink, it is important to understand their real-world sensing performance.

The term ‘sensing’ in sidelink V2X encompasses not only traditional radar-like functions (e.g., mapping of landmarks, tracking of moving objects) but also positioning of connected users [4], which is the focus of this work. Research in positioning can be broken down into *snapshot positioning* [11]–[16] and *tracking* [17]–[20], where the former considers a single time step, while the latter considers tracking of moving users over time, taking into account their motion models. Several studies

have explored V2X sidelink positioning within sub-6 GHz frequencies. For instance, [11] offers a comprehensive overview of V2X positioning, highlighting the synchronization limitations of time-difference-of-arrival (TDoA) methods and proposing the utilization of carrier phase and multipath information. Different positioning systems and architectures tailored for vehicular applications, along with relevant key performance indicators (KPIs) are described in [12]. A dynamic method for switching between global navigation satellite system (GNSS) and NR V2X TDoA measurements is presented in [13]. Additionally, [14] enhances positioning accuracy by combining vehicle-to-vehicle (V2V) range and angle measurements with vehicle-to-infrastructure (V2I) TDoA measurements. In [15], [16], the V2X sidelink positioning problem is investigated from an end-to-end perspective, and its theoretical performance bounds are derived. Regarding tracking in FR1, [17] demonstrates the viability of tracking by employing time-of-arrival (ToA) and angle-of-arrival (AoA) estimates in dense networks. This is achieved using cascaded extended Kalman filters (EKFs), where two EKFs are employed for tracking both the channel parameters of the propagation path corresponding to the largest power and the user. Notably, channel estimation is not implemented in this approach. Additionally, in [18], a neural network architecture is presented, enabling joint learning of user locations over time and the surrounding environment in an unsupervised manner. This approach utilizes time of flights, obtained using the MUSIC algorithm from received signals. Furthermore, [19] conducts tracking using an EKF, which utilizes received signal strengths from many known nodes as measurements. In [20], antenna-level carrier phase measurements are harnessed within an EKF framework to continuously track users’ 3D orientation and location. Synchronizing reference nodes in sidelink communication poses challenges, making solutions relying on a single reference node preferable. Surprisingly, there is limited research addressing the V2X sidelink tracking issue with a single reference node in FR1 from a standard end-to-end perspective.

In this paper, we investigate V2X sidelink tracking in FR1, employing a *comprehensive end-to-end methodology*. This approach incorporates ray-tracing-based channel modeling, a high-resolution channel estimator, and a Kalman filter (KF)-based tracking filter. Our primary contributions are summarized as follows: (i) We propose a novel method for estimating the measurement covariance, which is utilized in the update step of

the tracking filter, by computing the estimated error covariance lower bounds (EECLBs). (ii) We develop a gating method that utilizes tracking information to assist line-of-sight (LoS) identification. (iii) We validate the effectiveness of the end-to-end tracking framework using realistic ray-tracing data.

Notations: Scalars (e.g., x) are denoted in italic, vectors (e.g., \mathbf{x}) in bold, matrices (e.g., \mathbf{X}) in bold capital letters. Transpose is denoted by $(\cdot)^\top$. The Kronecker product is denoted by \otimes . A Gaussian density with mean \mathbf{u} and covariance Σ , evaluated in value \mathbf{x} is denoted by $\mathcal{N}(\mathbf{x}; \mathbf{u}, \Sigma)$. A n -by- n identical matrix is denoted by \mathbf{I}_n , and a n -by- n zero matrix is denoted by $\mathbf{0}_n$.

II. SYSTEM MODEL

In this paper, a sub-6 GHz V2X sidelink scenario involving a single fixed road-side unit (RSU) and a single moving connected road user (CRU) is examined. This section outlines the state models for both the RSU and the CRU, as well as the signal and measurement models.

A. State Models

In the considered scenario, the fixed RSU is equipped with a uniform rectangular array (URA). With respect to the global reference coordinate system, the center of the URA is located at $\mathbf{x}_{\text{RSU}} = [x_{\text{RSU}}, y_{\text{RSU}}, z_{\text{RSU}}]^\top$, and its orientation is described by Euler angles $\psi_{\text{RSU}} = [\varepsilon_{\text{RSU}}, \nu_{\text{RSU}}, \gamma_{\text{RSU}}]^\top$, ordered as roll, pitch, and yaw, respectively. Consequently, the state of the RSU is represented as $\mathbf{s}_{\text{RSU}} = [\mathbf{x}_{\text{RSU}}^\top, \psi_{\text{RSU}}^\top]^\top$, which remains constant over time and is assumed to be known a priori. The CRU is equipped with a single antenna, positioned at $\mathbf{x}_{\text{CRU},k} = [x_{\text{CRU},k}, y_{\text{CRU},k}, z_{\text{CRU},k}]^\top$ at time step k . The CRU moves over time, with a velocity $\dot{\mathbf{x}}_{\text{CRU},k} = [\dot{x}_{\text{CRU},k}, \dot{y}_{\text{CRU},k}, \dot{z}_{\text{CRU},k}]^\top$ at time step k and corresponding period T . Consequently, the state of the CRU at time step k is encapsulated by $\mathbf{s}_{\text{CRU},k} = [\mathbf{x}_{\text{CRU},k}^\top, \dot{\mathbf{x}}_{\text{CRU},k}^\top]^\top$, which evolves according to a predetermined dynamic model given by [21, Ch. 13.1]

$$\mathbf{s}_{\text{CRU},k} = \mathbf{F}\mathbf{s}_{\text{CRU},k-1} + \mathbf{G}\mathbf{n}_k, \quad (1)$$

where $\mathbf{F} \in \mathbb{R}^{6 \times 6}$ represents the transition matrix, $\mathbf{G} \in \mathbb{R}^{6 \times 2}$ and \mathbf{n}_k refers to the acceleration process noise, modeled as a zero-mean Gaussian noise with covariance $\mathbf{Q} = \sigma_a^2 \mathbf{I}_2$, such that $\mathbf{n}_k \sim \mathcal{N}(\mathbf{n}_k; \mathbf{0}, \mathbf{Q})$. Therefore, the transition density can be characterized as

$$p(\mathbf{s}_{\text{CRU},k} | \mathbf{s}_{\text{CRU},k-1}) = \mathcal{N}(\mathbf{s}_{\text{CRU},k}; \mathbf{F}\mathbf{s}_{\text{CRU},k-1}, \mathbf{G}\mathbf{Q}\mathbf{G}^\top). \quad (2)$$

B. Signal Model

We follow a round-trip-time (RTT) protocol in this paper. Every time step, the RSU sends orthogonal frequency-division multiplexing (OFDM) downlink pilot signals to the CRU, comprising N_{OFDM} symbols over S subcarriers. These signals can reach the CRU via the LoS path, which is the path that signals reach CRU directly and non-line-of-sight (NLoS) paths which are the paths that signals bounce off landmarks in the environment and then reach the CRU. The CRU responds with signals to the RSU following the RTT protocol. Additionally, we make the assumption that the transmission interval is sufficiently short to neglect any Doppler-induced phase effects. Consequently, the

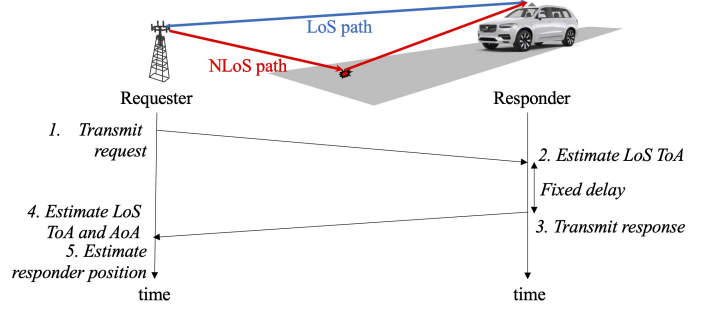


Fig. 1. The considered RTT protocol between a requester (a RSU) and a responder (a CRU).

received signal at time step k for the g -th OFDM symbol at the κ -th subcarrier can be expressed as [22]

$$\mathbf{y}_{\kappa,g,k} = \sum_{i=0}^{I_k-1} \rho_k^i \mathbf{a}(\boldsymbol{\theta}_k^i) e^{-j2\pi\kappa\Delta_f\tau_k^i} x_{\kappa,g} + \boldsymbol{\omega}_{\kappa,g,k}, \quad (3)$$

where $x_{\kappa,g}$ is the pilot signal, $\mathbf{y}_{\kappa,g,k}$ is the received signal across the RSU array, $\boldsymbol{\omega}_{\kappa,g,k}$ is the additive white Gaussian noise (AWGN), Δ_f is the subcarrier spacing, and $\mathbf{a}(\cdot)$ is the steering vectors of the RSU antenna arrays. There are I_k paths from landmarks in the environment at time step k with $i = 0$ representing the LoS path. Each path i can be described by a complex gain ρ_k^i , a ToA τ_k^i , and an AoA pair $\boldsymbol{\theta}_k^i = [\theta_{\text{az},k}^i, \theta_{\text{el},k}^i]^\top$ in azimuth and elevation. Please note that the signal model (3) is valid for both the RSU and CRU sides when acting as a receiver. The AoA pair $\boldsymbol{\theta}_k^i$ is determined by the direction of the signals that arrive the receiver (RSU or CRU) for the i -th path, and the ToA τ_k^i is determined by the propagation distance of the i -th path and a clock offset between the transmitter and the receiver (cancelled out through the RTT protocol).

The LoS AoA $\boldsymbol{\theta}_k^0$ at the RSU can be directly related to $\mathbf{x}_{\text{CRU},k}$ (see [16]), but the LoS ToA is given by $\tau_k^0 = \|\mathbf{x}_{\text{RSU}} - \mathbf{x}_{\text{CRU},k}\|/c + b_{\text{CRU},k}$, which depends on an unknown time-varying clock bias $b_{\text{CRU},k}$ between the RSU and CRU. Here c denotes the speed of light. To avoid tracking this bias, we utilize the RTT protocol, which is often used in range-based positioning to deal with the clock offset [7], [23]. As shown in Fig. 1, the RSU can measure the RTT to the CRU and infer the distance by subtracting the known processing time at the CRU.

C. Measurement Model

A channel estimator (see Section III-C1) will be applied on (3) to recover the channel parameters, i.e., gain, ToA and AoA. Channel parameters provided by the channel estimator at time step k are denoted by $\mathcal{G}_k = \{\mathbf{g}_k^0, \dots, \mathbf{g}_k^{\hat{I}_k-1}\}$, $\forall l \in \{0, \dots, \hat{I}_k - 1\}$, with $\mathbf{g}_k^l = [\hat{\rho}_k^l, \hat{\tau}_k^l, (\hat{\boldsymbol{\theta}}_k^l)^\top]^\top$ denoting an estimated path. In general, $\hat{I}_k \neq I_k$, since (i) not all paths can be resolved and some paths may be missed (including the LoS path); (ii) extra entries could be introduced in \mathcal{G}_k due to noise peaks during channel estimation. Hence, neither the existence of the LoS in \mathcal{G}_k nor the index of that path is known.

To track the CRU using the LoS path, we determine the LoS path in \mathcal{G}_k and convert it to a position estimate with an

associated measurement covariance. Hence, we directly use the estimated position as measurement, which is denoted as \mathbf{z}_k at time k . Consequently, we have the measurement function as

$$\mathbf{z}_k = \mathbf{H} \mathbf{s}_{\text{CRU},k} + \mathbf{r}_k, \quad (4)$$

where \mathbf{H} is the observation matrix describing the measurement function from $\mathbf{s}_{\text{CRU},k}$ to \mathbf{z}_k . Since \mathbf{z}_k is the measurement of CRU position $\mathbf{x}_{\text{CRU},k}$ only, $\mathbf{H} = [\mathbf{I}_3, \mathbf{0}_3]$. Moreover, \mathbf{r}_k refers to the measurement noise, modeled as a zero-mean Gaussian noise with covariance \mathbf{R}_k , such that $\mathbf{r}_k \sim \mathcal{N}(\mathbf{r}_k; \mathbf{0}, \mathbf{R}_k)$. Therefore, the likelihood can be described as

$$p(\mathbf{z}_k | \mathbf{s}_{\text{CRU},k}) = \mathcal{N}(\mathbf{z}_k; \mathbf{H} \mathbf{s}_{\text{CRU},k}, \mathbf{R}_k). \quad (5)$$

III. END-TO-END METHODOLOGY

To solve the CRU tracking problem, the formulation provided in (2) and (5) aligns well with a KF approach. In this section, we will detail the KF and its challenges in this application. To address these challenges, we utilize the EECLBs (introduced in Section III-B) as the measurement covariance \mathbf{R}_k , and the predicted density $\mathcal{N}(\mathbf{s}_{\text{CRU},k}; \mathbf{m}_{k|k-1}, \mathbf{P}_{k|k-1})$ is used to improve the LoS identification (introduced in Section III-C2).

A. Tracking Filter

The problem of estimating $\mathbf{s}_{\text{CRU},k}$ over time through noisy measurements $\mathbf{z}_{1:k}$ can be posed as a Bayesian filtering problem. The KF offers a closed-form solution to the Bayesian filtering equations when dealing with linear Gaussian dynamic and measurement models [21, Ch. 7.1]. As all predicted and posterior densities are Gaussian, we denote the predicted and posterior densities at time step k as

$$\begin{aligned} f(\mathbf{s}_{\text{CRU},k} | \mathbf{s}_{\text{CRU},k-1}, \mathbf{z}_{1:k-1}) &= \mathcal{N}(\mathbf{s}_{\text{CRU},k}; \mathbf{m}_{k|k-1}, \mathbf{P}_{k|k-1}), \\ f(\mathbf{s}_{\text{CRU},k} | \mathbf{z}_{1:k}) &= \mathcal{N}(\mathbf{s}_{\text{CRU},k}; \mathbf{m}_{k|k}, \mathbf{P}_{k|k}), \end{aligned}$$

with $\mathbf{m}_{k|k-1}$ and $\mathbf{P}_{k|k-1}$ denoting the mean and the covariance of $f(\mathbf{s}_{\text{CRU},k} | \mathbf{s}_{\text{CRU},k-1}, \mathbf{z}_{1:k-1})$, and $\mathbf{m}_{k|k}$, and $\mathbf{P}_{k|k}$ denoting the mean and the covariance of $f(\mathbf{s}_{\text{CRU},k} | \mathbf{z}_{1:k})$. The predicted and posterior density parameters are [21, Ch. 7.1]:

- *Prediction step:* The predicted mean and covariance are

$$\mathbf{m}_{k|k-1} = \mathbf{F} \mathbf{m}_{k-1|k-1}, \quad (6)$$

$$\mathbf{P}_{k|k-1} = \mathbf{F} \mathbf{P}_{k-1|k-1} \mathbf{F}^\top + \mathbf{G} \mathbf{Q} \mathbf{G}^\top. \quad (7)$$

- *Update step:* From the measurement \mathbf{z}_k , the updated mean and covariance are obtained as

$$\hat{\mathbf{z}}_k = \mathbf{H} \mathbf{m}_{k|k-1}, \quad (8)$$

$$\mathbf{S}_k = \mathbf{H} \mathbf{P}_{k|k-1} \mathbf{H}^\top + \mathbf{R}_k, \quad (9)$$

$$\mathbf{K}_k = \mathbf{P}_{k|k-1} \mathbf{H}^\top \mathbf{S}_k^{-1}, \quad (10)$$

$$\mathbf{m}_{k|k} = \mathbf{m}_{k|k-1} + \mathbf{K}_k (\mathbf{z}_k - \hat{\mathbf{z}}_k), \quad (11)$$

$$\mathbf{P}_{k|k} = \mathbf{P}_{k|k-1} - \mathbf{K}_k \mathbf{H} \mathbf{P}_{k|k-1}, \quad (12)$$

where $(\mathbf{z}_k - \hat{\mathbf{z}}_k)$, \mathbf{S}_k and \mathbf{K}_k are usually referred as the innovation, innovation covariance, and Kalman gain, respectively. Note that the update step is skipped if no measurement arrives, i.e., the channel estimator does not provide an estimation of the LoS path.

The recursion begins with the mean $\mathbf{m}_{0|0}$ and the covariance $\mathbf{P}_{0|0}$ of the prior density $f(\mathbf{s}_{\text{CRU},0})$.

The main challenges of implementing the tracking filter under the considered FR1 scenario are as follows:

- *Measurement covariance estimation:* The measurement covariance \mathbf{R}_k reflects the quality of the measurement and affects how much the tracking filter should believe in the measurement. However, \mathbf{R}_k is not directly available in the considered problem as the receiver only has access to (3). Therefore, a good estimation on \mathbf{R}_k is essential to have good tracking performance.
- *LoS identification:* Channel estimator provides a group of estimated paths every time step. We do not know if the LoS path is part of \mathcal{G}_k , nor what its index is. Hence, we should identify which is the estimation of the LoS path and use the position estimate from it as the measurement. The estimated path with the shortest delay is usually chosen as the LoS path. However, this method can lead to large errors since the shortest estimated path does not always correspond to the LoS path.

B. Measurement Noise Covariance Estimation

In this section, the fundamentals of Fisher Information Matrix (FIM) are briefly introduced, and two proposed EECLB to estimate \mathbf{R}_k are described.

1) *FIM:* FIM offers a prevalent method for assessing the performance of estimation algorithms in statistical estimation theory, indicating the mean squared error (MSE) of any unbiased estimator should always be larger than the inverse of the FIM [24, Ch. 4.2]. Suppose we have a measurement model $\psi = \boldsymbol{\mu}(\boldsymbol{\eta}, \boldsymbol{\kappa}) + \boldsymbol{\varpi}$, with $\boldsymbol{\varpi}$ denoting a complex white noise with variance N_0 , $\boldsymbol{\mu}(\cdot)$ denoting a known possibly non-linear mapping, $\boldsymbol{\eta}$ denoting the parameters of interest, and $\boldsymbol{\kappa}$ denoting the nuisance parameters. The lower bound on the estimation error of $\boldsymbol{\xi} = [\boldsymbol{\eta}^\top, \boldsymbol{\kappa}^\top]^\top$ has the form

$$\mathbb{E}\{(\boldsymbol{\xi} - \hat{\boldsymbol{\xi}})((\boldsymbol{\xi} - \hat{\boldsymbol{\xi}})^\top)\} \succeq \boldsymbol{\Xi}^{-1}(\boldsymbol{\xi}), \quad (13)$$

where $\hat{\boldsymbol{\xi}}$ denotes an estimate of $\boldsymbol{\xi}$, and $\boldsymbol{\Xi}(\boldsymbol{\xi})$ is the FIM of $\boldsymbol{\xi}$ given by

$$\boldsymbol{\Xi}(\boldsymbol{\xi}) = \frac{2}{N_0} \Re\left\{ \left(\frac{\partial \boldsymbol{\mu}(\boldsymbol{\xi})}{\partial \boldsymbol{\xi}} \right)^\text{H} \frac{\partial \boldsymbol{\mu}(\boldsymbol{\xi})}{\partial \boldsymbol{\xi}} \right\}, \quad (14)$$

with $\partial \boldsymbol{\mu}(\boldsymbol{\xi}) / \partial \boldsymbol{\xi}$ denoting the gradient matrix. The inequality in (13) indicates that the MSE of an estimator is larger than $\boldsymbol{\Xi}^{-1}$ in the positive semidefinite sense. The error covariance lower bound (ECLB) of $\boldsymbol{\eta}$ can be obtained by taking the corresponding sub-matrix of $\boldsymbol{\Xi}^{-1}(\boldsymbol{\xi})$, i.e., $\text{ECLB}(\boldsymbol{\eta}) = [\boldsymbol{\Xi}^{-1}(\boldsymbol{\xi})]_{1:\text{dim}(\boldsymbol{\eta}), 1:\text{dim}(\boldsymbol{\eta})}$, where $\text{dim}(\cdot)$ returns the dimension of the argument.

2) *Measurement Covariance Estimation:* We use estimates of the ECLB of the CRU position to estimate the measurement noise covariance. As only the LoS paths are used in this problem, we compute the ECLB in two steps. Firstly, we compute the ECLB of $\boldsymbol{\eta} = [\tau_k^0, (\boldsymbol{\theta}_k^0)^\top]^\top$ related to the observation (3) according to (14) every time step. Secondly, the ECLB of the CRU position can be computed using a standard Jacobian approach, as the $[\tau_k^0, (\boldsymbol{\theta}_k^0)^\top]^\top$ is a function of $\mathbf{x}_{\text{CRU},k}$. However, computing the ECLB requires knowing the ground-truth channel parameters and the ground-truth CRU position, which are not

available in real implementation. To estimate the ECLB, we view the estimated paths \mathcal{G}_k provided by the channel estimator and the predicted mean of the CRU state $\mathbf{m}_{k|k-1}$ as ground-truth, and use these values into ECLB computation. Similar to the LoS and the NLoS bounds in [16], we compute the estimations of two ECLBs:

- *ECLB based on the estimated LoS parameters:* only the LoS path in \mathcal{G}_k is utilized in (3), in both links of the RTT protocol. The resulting estimated ECLB (EECLB) is denoted by EECLB-LOS.
- *ECLB based on the estimated LoS and NLoS parameters:* all paths in \mathcal{G}_k are utilized in (3), in both links of the RTT protocol. Given that paths outside the resolution cell of the LoS path do not impact the estimation accuracy of the LoS path, we omit these paths when computing the ECLB. The resulting EECLB is denoted by EECLB-NLOS.

These EECLBs are directly used as \mathbf{R}_k in the tracking filter. Please note if there is no estimate within \mathcal{G}_k corresponding to the LoS path, then neither of the two EECLBs exists.

C. LoS Identification

To understand the LoS identification, we first describe the channel parameter estimator, which generates \mathcal{G}_k from (3).

1) *Channel Parameter Estimation:* We describe the high-resolution channel estimation algorithm used to infer the geometric path parameters (i.e., gain, delay and AoA) using the observations in (3). In (3), we wipe off the constant modulus pilots $x_{\kappa,g}$ via conjugate multiplication and coherently integrate over N_{OFDM} symbols, assuming short transmission interval (i.e., Doppler-induced phases are ignored). Then, (3) can be reformulated as a 3-D tensor $\mathcal{Y}_k \in \mathbb{C}^{N_z \times N_x \times S}$

$$\mathcal{Y}_k = \sum_{i=0}^{I_k-1} \rho_k^i \mathbf{a}_z(\theta_k^i) \circ \mathbf{a}_x(\theta_k^i) \circ \mathbf{d}(\tau_k^i) + \mathcal{N}_k, \quad (15)$$

where \circ denotes the outer product and integration gains are absorbed in ρ_k^i . In (15), the horizontal and vertical spatial-domain steering vectors, $\mathbf{a}_x(\theta) \in \mathbb{C}^{N_x \times 1}$ and $\mathbf{a}_z(\theta) \in \mathbb{C}^{N_z \times 1}$, are defined, respectively, as

$$[\mathbf{a}_x(\theta)]_n = e^{j\frac{2\pi}{\lambda} d_x n \cos(\theta_{e1}) \sin(\theta_{az})}, [\mathbf{a}_z(\theta)]_n = e^{j\frac{2\pi}{\lambda} d_z n \sin(\theta_{e1})},$$

where d_x and d_z denote the element spacing, N_x and N_z are the number of antenna elements in the horizontal and vertical axes of the URA, and $\mathbf{a}(\theta) = \mathbf{a}_x(\theta) \otimes \mathbf{a}_z(\theta)$. In addition, $\mathbf{d}(\tau) \in \mathbb{C}^{S \times 1}$ represents the frequency-domain steering vector with $[\mathbf{d}(\tau)]_\kappa = e^{-j2\pi\kappa\Delta_f\tau}$ and \mathcal{N}_k is the noise tensor.

To estimate the path parameters from (15), we employ a tensor decomposition based high-resolution channel estimation algorithm [16]. We first construct a new tensor $\tilde{\mathcal{Y}}_k \in \mathbb{C}^{N_z(n_z+1) \times N_x(n_x+1) \times V}$ (where $V = S - n_z - n_x$) from the original tensor observation in (15) by augmenting the spatial domain with the frequency domain measurements [16, Eq. (15)] to deal with the rank deficiency problem in standard CP decomposition (CPD)-based channel estimation. After applying this spatial augmentation (SA) strategy, we have

$$\tilde{\mathcal{Y}}_k = \sum_{i=0}^{I_k-1} \rho_k^i \tilde{\mathbf{a}}_z(\theta_k^i, \tau_k^i) \circ \tilde{\mathbf{a}}_x(\theta_k^i, \tau_k^i) \circ \tilde{\mathbf{d}}(\tau_k^i) + \tilde{\mathcal{N}}_k \quad (16)$$

where

$$\tilde{\mathbf{a}}_z(\theta, \tau) = \mathbf{a}_z(\theta) \otimes [\mathbf{d}(\tau)]_{1:n_z+1} \in \mathbb{C}^{N_z(n_z+1) \times 1}, \quad (17a)$$

$$\tilde{\mathbf{a}}_x(\theta, \tau) = \mathbf{a}_x(\theta) \otimes [\mathbf{d}(\tau)]_{1:n_x+1} \in \mathbb{C}^{N_x(n_x+1) \times 1}, \quad (17b)$$

$$\tilde{\mathbf{d}}(\tau) = [\mathbf{d}(\tau)]_{1:V} \in \mathbb{C}^{V \times 1}. \quad (17c)$$

Next, we apply CPD to $\tilde{\mathcal{Y}}_k$ in (16), i.e.,

$$\min_{\{\mathbf{a}_z^i, \mathbf{a}_x^i, \mathbf{d}^i\}_{i=0}^{I_k-1}} \|\tilde{\mathcal{Y}} - \tilde{\mathcal{Y}}_k\|_F^2 \quad (18a)$$

$$\text{s.t. } \hat{\mathcal{Y}} = \sum_{i=0}^{I_k-1} \mathbf{a}_z^i \circ \mathbf{a}_x^i \circ \mathbf{d}^i. \quad (18b)$$

Based on (17), the parameters of the I_k paths at time step k can be estimated from the output of (18) using

$$\hat{\tau}_k^i = -\frac{\angle([\mathbf{J}_1 \mathbf{d}^i]^H [\mathbf{J}_2 \mathbf{d}^i])}{2\pi\Delta_f}, \quad (19a)$$

$$\hat{\theta}_{e1,k}^i = \arg \max_{\theta_{e1}} |(\mathbf{a}_z^i)^H \tilde{\mathbf{a}}_z(\theta, \hat{\tau}_k^i)|^2, \quad (19b)$$

$$\hat{\theta}_{az,k}^i = \arg \max_{\theta_{az}} |(\mathbf{a}_x^i)^H \tilde{\mathbf{a}}_x(\theta_{az}, \hat{\theta}_{e1,k}^i, \hat{\tau}_k^i)|^2, \quad (19c)$$

and $\hat{\rho}_k = \mathbf{B}_k^\dagger \check{\mathcal{Y}}_k$, where \mathbf{J}_1 and \mathbf{J}_2 are selection matrices selecting the first and the last $V-1$ elements of a given right-multiplying vector, $\mathbf{B}_k \in \mathbb{C}^{N_z N_x S \times I_k}$ whose i -th column is given by $[\mathbf{B}_k]_{:,i} = \mathbf{d}(\hat{\tau}_k^i) \otimes \mathbf{a}_x(\hat{\theta}_{az,k}^i, \hat{\theta}_{e1,k}^i) \otimes \mathbf{a}_z(\hat{\theta}_{az,k}^i, \hat{\theta}_{e1,k}^i)$, $\check{\mathcal{Y}}_k = \text{vec}(\mathcal{Y}_k) \in \mathbb{C}^{N_z N_x S \times 1}$, $\hat{\rho}_k \in \mathbb{C}^{I_k \times 1}$ with $[\hat{\rho}_k]_i = \hat{\rho}_k^i$ denoting the estimate of the path gain ρ_k^i in (15), and $(\cdot)^\dagger$ denotes Moore-Penrose pseudo-inverse.

2) *Tracking-aided LoS Identification:* At time step k , we view the predicted CRU position in (6) as the ground-truth position. From this, we reconstruct τ_k^0 and θ_k^0 , denoted as $\check{\mathbf{q}}_k = [\tau_k^0, (\theta_k^0)^\top]^\top$. Subsequently, we define a range-angle gate centered around $\check{\mathbf{q}}_k$, with the spread determined by $\mathbf{P}_{k|k-1}$, i.e.,

$$\mathcal{H}_k = \{\mathbf{q} \mid (\mathbf{q} - \check{\mathbf{q}}_k)^\top (\mathbf{U}_k)^{-1} (\mathbf{q} - \check{\mathbf{q}}_k) \leq \beta\}, \quad (20)$$

where β is the gating threshold, $\mathbf{U}_k = \mathbf{M}_k \mathbf{P}_{k|k-1} \mathbf{M}_k^\top$ approximates the covariance of $\check{\mathbf{q}}_k$ with \mathbf{M}_k denoting the Jacobian from the predicted position to $\check{\mathbf{q}}_k$. Using the gate defined in (20), the detection of LoS occurs if at least one of the estimated paths falls within the gate \mathcal{H}_k . Then, among those paths, the one with the closest ToA to τ_k^0 is selected as the LoS path. If no LoS path is found, the update step in the KF is skipped.

IV. SIMULATIONS

A. Simulation Environment

We adhere to the 3GPP RSU deployment procedure according to [25]. We focus on an urban vehicular scenario situated at an intersection, depicted in Fig. 2, and simulate it using the REMCOM Wireless InSite@ray-tracer [26]. The RSU is located at the center of the intersection, precisely at coordinates $[0 \text{ m}, 0 \text{ m}, 10 \text{ m}]^\top$. Surrounding the intersection are four buildings, with their centers located at $[\pm 45 \text{ m}, \pm 45 \text{ m}, 15 \text{ m}]^\top$, respectively, and all measuring 50 m in length, 50 m in width, and 30 m in height. The ground material is concrete, while the buildings feature brick walls. The RSU is equipped with a 2×4 antenna array, and the CRU is deployed with a single antenna, following the antenna patterns specified in [16]. The CRU possesses an initial velocity along the y-axis, and travels on the

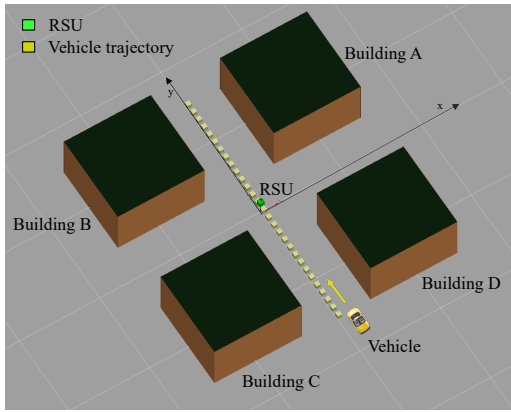


Fig. 2. The ray-tracing simulation environment with a single RSU at the center of the intersection, four buildings, and a vehicle moving from down to up.

ground alongside the lane, with its antenna positioned at a height of 1.5 m. The center of lane extends from $[1.6 \text{ m}, -70 \text{ m}, 0 \text{ m}]^T$ to $[1.6 \text{ m}, 70 \text{ m}, 0 \text{ m}]^T$.

In terms of signal parameters, the carrier frequency is set at 5.9 GHz. The OFDM pilot signals consist of 12 symbols, each maintaining a constant amplitude. The total active bandwidth spans 17.28 MHz, distributed over 288 subcarriers with a subcarrier spacing of 60 kHz. The transmit power is configured to 10 dBm, the noise spectral density stands at -174 dBm/Hz , and the receiver noise figure is set at 8 dB. Measurements are generated every 100 ms. Additionally, we assume a 2D constant velocity model for (2), with $\sigma_a = 0.1 \text{ m/s}^2$ and $T = 10 \text{ ms}$. Despite the scenario being 3D, we operate in a 2D context, as the CRU traverses the ground and maintains its antenna height fixed at 1.5 m.

We assess the tracking performance by computing the root mean squared error (RMSE) of the CRU position estimates across 100 Monte Carlo (MC) simulations or cumulative density functions (CDFs) of absolute errors. In each simulation, we first generate propagation paths using the raytracing data, then employ the channel estimator introduced in Section III-C1 on the generated signals to acquire channel parameters. Subsequently, we derive a position estimate from the identified LoS path and apply the tracking filter to track the CRU over time. We compare RMSE performances using EECLB-LOS and EECLB-NLOS as measurement covariance against four benchmarks (BMs): **BM1: tracking using non-stationary MSE** as the measurement covariance (namely tracking, non-stat.), which is the *instantaneous* position MSE estimated across 100 MC simulations for each time step/location; **BM2: tracking using stationary MSE** as the measurement covariance (namely tracking, stat.), which is the *average* position MSE, i.e., averaged across 100 MC simulations and across all time steps/locations; **BM3: snapshot positioning** (position estimates from the identified LoS paths *without any tracking*), and **BM4: dead reckoning** (pure integration *without considering measurements*). Later, we will also compare tracking performances of EECLB-LOS and EECLB-NLOS in cases with and without gating.

B. Results and Discussion

We begin by examining the viability of the tracking filter employing the proposed covariance estimates. Fig. 3 shows the

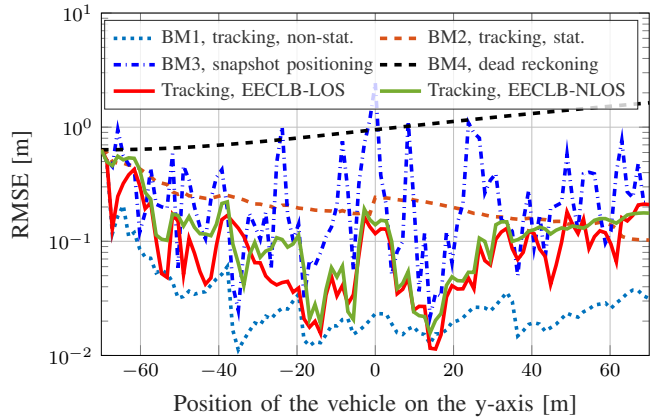


Fig. 3. Comparison of tracking performances when EECLB-LOS and EECLB-NLOS are used as the measurement covariance in the tracking filter with four benchmarks. Here, gating is not implemented in LoS identification.

tracking results using EECLB-LOS and EECLB-NLOS as the measurement covariance, compared against four benchmarks, where the gating is not implemented. Our observations indicate that the tracking filter performs admirably, generally showcasing lower RMSEs compared to the snapshot positioning and dead reckoning results, regardless of the covariance used in four tracking results. This superior performance is attributed to the tracking filter's incorporation of both measurements and CRU motion, which leads to enhanced accuracy. In contrast, snapshot positioning disregards CRU motion, and dead reckoning overlooks measurements entirely. Among the four tracking results, the optimal performance is achieved when utilizing the non-stationary MSE, as it accurately reflects the true quality of the measurement, whereas the EECLB-LOS, the EECLB-NLOS and the stationary MSE serve merely as estimates of the measurement covariance. Furthermore, the least satisfactory performance is observed when utilizing the stationary MSE as the covariance. This is due to the covariance remaining static, thereby unable to accommodate fluctuations in measurement quality across time/space. When employing the EECLB-LOS, the tracking filter exhibits better performance compared to employing EECLB-NLOS. This discrepancy arises from the fact that all paths within \mathcal{G}_k are already resolved by the channel estimator. However, resolved NLoS paths falling within the resolution cell of the estimated LoS paths introduce errors in ECLB estimation, resulting in degraded tracking performance.

Next, we investigate how gating enhances the tracking performance by aiding the LoS identification. Fig. 4 displays RMSEs of ToA estimates for the LoS path in both gating and non-gating cases. The lower RMSE in the gating case is attributed to the correct identification of the LoS path among the detected paths with gating assistance. The discontinuities observed in the solid line, e.g. around $y = 24 \text{ m}$ in Fig. 4, correspond to instances where no LoS measurements are identified (i.e., no measurements fall within the LoS gate). In such instances, the dashed line generally exhibits larger errors, because of incorrect identification of the LoS path among the detected paths. We also examine the CDFs of the absolute positioning error for the tracking results using two EECLBs, in cases with and without

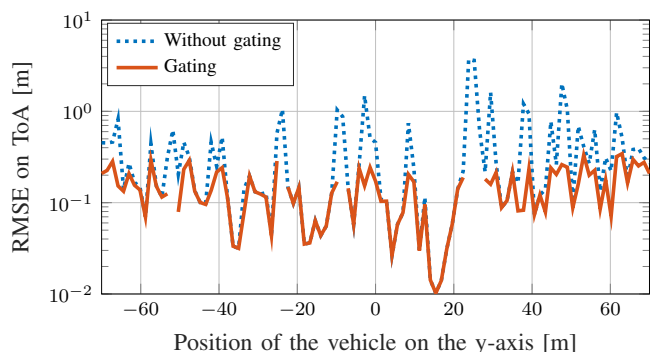


Fig. 4. Comparison of the RMSEs of ToA estimates for the LoS path in both cases, with and without gating.

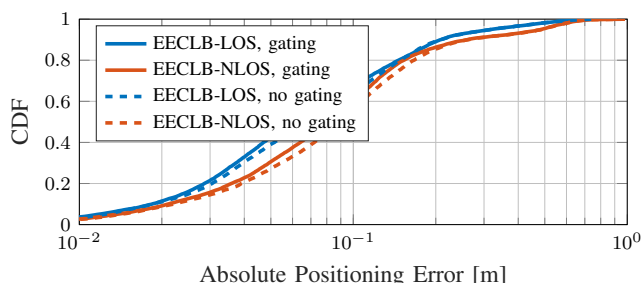


Fig. 5. Comparison of tracking performances when EECLB-LOS and EECLB-NLOS are used as the measurement covariance in the update step of the tracking filter in both cases, with and without gating.

implementing gating, as illustrated in Fig. 5. Improved tracking outcomes are observed in both cases when either the EECLB-LOS or EECLB-NLOS is used, as indicated by the dashed lines positioned to the right of the solid lines in Fig. 5. This improvement stems from the correct identification of the LoS path among the detected paths in certain instances facilitated by gating. Conversely, without gating, the LoS path is often misidentified.

V. CONCLUSIONS

In this paper, our focus lies on addressing the V2X sidelink tracking problem within the framework of 3GPP Release 18 in sub-6 GHz. Our objective is to track the trajectory of a moving CRU over time, aided by a single RSU. We develop a tracking filter based on the KF, wherein two EECLBs are employed as the measurement covariance in the update step of the tracking filter. Additionally, we introduce a gating method wherein the intermediate tracking results are leveraged to enhance LoS identification. To evaluate the efficacy of our approach, we conduct simulations in an urban scenario at an intersection using ray-tracing data. Our results demonstrate that the tracking filter, coupled with the proposed EECLBs, exhibits satisfactory performance, albeit with a discernible gap compared to the case employing the non-stationary MSE. Furthermore, our results underscore the efficacy of the proposed gating method in improving overall tracking performance by enabling more accurate identification of LoS paths among the detected paths.

ACKNOWLEDGMENTS

The authors wish to thank Remcom for providing Wireless InSite®ray-tracer.

REFERENCES

- [1] T. Wild, *et al.*, “Joint design of communication and sensing for beyond 5G and 6G systems,” *IEEE Access*, vol. 9, pp. 30 845–30 857, 2021.
- [2] F. Liu, *et al.*, “Integrated sensing and communications: Towards dual-functional wireless networks for 6G and beyond,” *IEEE JSAC*, 2022.
- [3] O. Kanhere *et al.*, “Position location for futuristic cellular communications: 5G and beyond,” *IEEE Communications Magazine*, vol. 59, no. 1, pp. 70–75, 2021.
- [4] H. Wymeersch *et al.*, “Localisation and sensing use cases and gap analysis,” Hexa-X project Deliverable D3.1, v1.4, 2022. [Online]. Available: <https://hexa-x.eu/deliverables/>
- [5] T. Wild, *et al.*, “6G integrated sensing and communication: From vision to realization,” in *European Radar Conference (EuRAD)*, 2023, pp. 355–358.
- [6] 3GPP, “Study on scenarios and requirements of in-coverage, partial coverage, and out-of-coverage NR positioning use cases,” TR 38.845, Technical Report 17.0.0, 2021.
- [7] H. Bagheri, *et al.*, “5G NR-V2X: Toward connected and cooperative autonomous driving,” *IEEE Communications Standards Magazine*, vol. 5, no. 1, pp. 48–54, 2021.
- [8] M. H. C. Garcia, *et al.*, “A tutorial on 5G NR V2X communications,” *IEEE Communications Surveys & Tutorials*, vol. 23, no. 3, pp. 1972–2026, 2021.
- [9] S.-Y. Lien, *et al.*, “3GPP NR sidelink transmissions toward 5G V2X,” *IEEE Access*, vol. 8, pp. 35 368–35 382, 2020.
- [10] 3GPP, “Study on expanded and improved NR positioning,” TR 38.859, Technical Report 0.1.0, 2022.
- [11] S.-W. Ko, *et al.*, “V2X-based vehicular positioning: Opportunities, challenges, and future directions,” *IEEE Wireless Communications*, vol. 28, no. 2, pp. 144–151, 2021.
- [12] Q. Liu, *et al.*, “A highly accurate positioning solution for C-V2X systems,” *Sensors*, vol. 21, no. 4, p. 1175, 2021.
- [13] A. Fouda, *et al.*, “Dynamic selective positioning for high-precision accuracy in 5G NR V2X networks,” in *IEEE Vehicular Technology Conference (VTC2021-Spring)*, 2021.
- [14] Q. Liu, *et al.*, “A V2X-integrated positioning methodology in ultradense networks,” *IEEE Internet of Things Journal*, vol. 8, no. 23, pp. 17 014–17 028, 2021.
- [15] Y. Ge, *et al.*, “Analysis of V2X sidelink positioning in sub-6 GHz,” in *IEEE International Symposium on Joint Communications & Sensing (JC&S)*, 2023, pp. 1–6.
- [16] Y. Ge, *et al.*, “V2X sidelink positioning in FR1: Scenarios, algorithms, and performance evaluation,” *IEEE Journal on Selected Areas in Communications*, 2024.
- [17] M. Koivisto, *et al.*, “Joint device positioning and clock synchronization in 5G ultra-dense networks,” *IEEE Transactions on Wireless Communications*, vol. 16, no. 5, pp. 2866–2881, 2017.
- [18] S. Kadambi, *et al.*, “Neural RF SLAM for unsupervised positioning and mapping with channel state information,” in *IEEE International Conference on Communications*, 2022, pp. 3238–3244.
- [19] P. T. Karfakis, *et al.*, “NR5G-SAM: A SLAM framework for field robot applications based on 5G new radio,” *Sensors*, vol. 23, no. 11, p. 5354, 2023.
- [20] J. Talvitie, *et al.*, “Orientation and location tracking of XR devices: 5G carrier phase-based methods,” *IEEE Journal of Selected Topics in Signal Processing*, 2023.
- [21] F. Gustafsson, *Statistical Sensor Fusion*. Studentlitteratur, 2010.
- [22] R. W. Heath, *et al.*, “An overview of signal processing techniques for millimeter wave MIMO systems,” *IEEE Journal of Selected Topics in Signal Processing*, vol. 10, no. 3, pp. 436–453, 2016.
- [23] S. Parkvall, *et al.*, “5G NR release 16: Start of the 5G evolution,” *IEEE Communications Standards Magazine*, vol. 4, no. 4, pp. 56–63, 2020.
- [24] H. L. Van Trees, *Detection, Estimation, and Modulation Theory, Part I: Detection, Estimation, and Linear Modulation Theory*. John Wiley & Sons, 2004.
- [25] 3GPP, “Technical specification group radio access network; study on evaluation methodology of new vehicle-to-everything (V2X) use cases for LTE and NR,” TR 37.885, Technical Report 15.3.0, 2019.
- [26] Remcom. Wireless InSite - 3D Wireless Prediction Software. Accessed: Oct 9, 2022). [Online]. Available: <https://www.remcom.com/wireless-insite-em-propagation-software>